공학석사 학위논문

EEG Spectro-spatial Pattern Related to Phenoconversion in Patients with REM Sleep Behavior Disorder

렘수면행동장애에서 질병전환과 관련된 뇌파 주파수-공간 패턴 규명

2023년 8월

서울대학교 대학원
협동과정 바이오엔지니어링전공

박경은

EEG Spectro-spatial Pattern Related to Phenoconversion in Patients with REM Sleep Behavior Disorder

지도 교수 정기영

이 논문을 공학석사 학위논문으로 제출함

2023년 8월

서울대학교 대학원

공과대학 협동과정 바이오엔지니어링전공

박경은

박경은의 공학석사 학위논문을 인준함

2023년 8월

위원장	김한준	(인)
부위원장	정기영	(인)
위원	신정환	(인)

Abstract

Objective: This study aimed to identify EEG spectro-spatial covariance patterns associated with phenoconversion in patients with isolated REM sleep behavior disorder (iRBD) and investigate the longitudinal trajectories in iRBD, Parkinson's disease (PD), and dementia with Lewy bodies (DLB) patients.

Methods: We obtained eye-closed resting EEG data at baseline and follow-up from 12 iRBD patients who later developed PD, 6 patients who later developed DLB, and 17 iRBD patients who did not convert. In the source space, we derived PD-RBD and DLB-RBD related patterns for each frequency band using EEG data collected after phenoconversion in iRBD converters, with 12 age- and sex-matched healthy control (HC) participants as the reference group. We analyzed correlations between pattern expression scores and motor and cognitive function measures. Additionally, we examined differences between iRBD converters and nonconverters at baseline. Finally, we observed the longitudinal trajectory of iRBD nonconverters, PD converters, and DLB converters in the combined pattern space.

Results: The delta and alpha spatial covariance patterns effectively distinguished both PD converters and DLB converters from HC, with the alpha pattern demonstrating the highest discriminative power (AUC = 0.9097 for PD-RBD pattern, 0.9306 for DLB-RBD pattern). MDS-UPDRS part III scores positively correlated with delta pattern scores (rho = 0.688, p = 0.00014 for PD-RBD pattern, and rho = 0.539, p = 0.0055 for DLB-RBD pattern), even after adjusting for age and sex. However, no significant correlation was found between MoCA-K scores and any of the pattern expression scores. At baseline, converters had higher scores for the PD-RBD and DLB-RBD beta2 pattern compared to nonconverters, but the two groups were not well distinguished (AUC = 0.7751, rank sum p = 0.0062). All three groups showed an overall rightward shift in the combined pattern space, with each group

exhibiting distinct trajectories.

Conclusions: PD-RBD and DLB-RBD EEG spectro-spatial covariance patterns can be utilized for early detection and monitoring of neurodegenerative disorders. The complementary use of patterns derived by other modalities may provide a better understanding.

Keyword : REM sleep behavior disorder; EEG; Alpha-synucleinopathy; Parkinson's disease; Dementia with Lewy bodies; Spatial covariance pattern.
Student Number : 2021-23744

Table of Contents

List of Tables

List of Figures

Abbreviations

REM, rapid eye movement

RBD, REM sleep behavior disorder

iRBD, isolated RBD

PD, Parkinson’s disease

DLB, dementia with Lewy bodies

MSA, multiple system atrophy

SSM/PCA, scaled subprofile model using principal component analysis

EEG, electroencephalography

AHI, apnea-hypopnea index

MDS-UPDRS, Movement Disorder Society-Sponsored Revision of the Unified Parkinson’s Disease Rating Scale

MoCA-K, Korean version of the Montreal Cognitive Assessment

HC, healthy controls

PD-RBD, iRBD patients who converted to PD

DLB-RBD, iRBD patients who converted to DLB

EOG, electrooculography

PSD, power spectral density

DOF, dominant occipital frequency

PC, principal component

AIC, Akaike Information Criterion

LOOCV, Leave-one-out cross-validation

ROC, receiver operating characteristic

AUC, area under the ROC curve

iRBD-NC, iRBD nonconverters

MCI, mild cognitive impairment

PDRP, PD related metabolic pattern

DLBRP, DLB related metabolic pattern

RBDRP, RBD related metabolic pattern

dnPDRBD, de novo PD patients with a history of RBD before developing parkinsonism

dnPDRBDRP, dnPDRBD related metabolic pattern

MRI, magnetic resonance imaging

Chapter 1. Introduction

Isolated Rapid eye movement (REM) sleep behavior disorder (iRBD) is prodromal stage of α-synucleinopathies, such as Parkinson's disease (PD), dementia with Lewy bodies (DLB) and multiple system atrophy (MSA).[1,2] More than 70% of iRBD patients eventually develop parkinsonism or dementia within 12 years follow-up.[1,3] Therefore, the identification of reliable biomarkers capable of predicting neurodegeneration in iRBD patients has become a matter of significant importance.

In recent research, investigations into disease-related spatial covariance patterns in neuroimaging have been carried out. Notably, several studies have applied Scaled Subprofile Model using principal component analysis (SSM/PCA) method to [^{18}F]FDG-PET imaging data to identify brain metabolic patterns associated with PD, DLB and REM sleep behavior disorder (RBD).[4-8] Additionally, the pattern expression level was found to be a predictive marker for future phenoconversion and its subtype, and also exhibited progressive changes as the disease advanced.[6,9,10]

However, it is crucial to acknowledge that while neuroimaging techniques, such as FDG-PET, offer detailed spatial images and valuable metabolic information, they come with certain limitations. FDG-PET involves radiation exposure and significant imaging costs, making it less feasible for widespread and repeated use.

In contrast, electroencephalography (EEG) offers a distinct set of advantages. It boasts high temporal resolution, allowing for precise monitoring of real-time neuronal activity and dynamic changes in brain function. Additionally, EEG is a non-invasive method, posing minimal risk to patients.

Notably, EEG slowing, characterized by an increase in delta and theta power and a lower dominant occipital frequency in the resting state, has been reported in iRBD and several neurodegenerative disorders, including PD and DLB.[11-14] This slowing of brain activity, often observed in α-synucleinopathies, offers a promising window to directly observe changes associated with phenoconversion using

EEG.

In light of these considerations, this study aims to leverage the unique benefits of EEG, such as high temporal resolution and cost-effectiveness, to identify and investigate spectro-spatial patterns associated with phenoconversion in patients with iRBD. By doing so, we hope to contribute valuable insights into the early detection and monitoring of neurodegenerative disorders and improve the understanding of the underlying mechanisms involved in the transition from iRBD to α-synucleinopathies.

Chapter 2. Methods

2.1. Participants

We prospectively recruited patients diagnosed with iRBD based on the third edition of the International Classification of Sleep Disorders at the Seoul National University Hospital between 2014 and 2022.[15] Patients with any neurological disease, psychiatric condition, severe medical illness, secondary RBD due to medication, or moderate to severe obstructive sleep apnea (apnea-hypopnea index (AHI) ≥ 15) in their current state or medical history were excluded from the study. Each patient underwent examination by two neurologists, JK (specialized in sleep disorders), and KH (specialized in movement disorders), to confirm the presence of sleep disorders and neurological diseases at baseline.

We utilized Movement Disorder Society-Sponsored Revision of the Unified Parkinson's Disease Rating Scale (MDS-UPDRS) part III and the Korean version of the Montreal Cognitive Assessment (MoCA-K) to assess motor and cognitive function, respectively. During the clinical follow-up period, annual assessments of MDS-UPDRS part III and MoCA-K were conducted. The evaluation of phenoconversion in iRBD patients was performed every 6 to 12 months based on standard criteria.[16-18] Patients who subsequently developed PD, DLB, or MSA from iRBD were categorized as iRBD converters, while those who did not undergo phenoconversion during the follow-up period were defined as iRBD nonconverters. Among iRBD converters, only patients who converted to PD (PD-RBD) and DLB (DLB-RBD) were included in the study. Age- and sex-matched healthy controls (HC) with MoCA-K scores above 23 were also recruited. This study was approved by the Institutional Review Board of Seoul National University Hospital (IRB No. 1406-100-589, 1708-169-883, 1507-100-689), and written informed consent was obtained from every participant.

2.2. EEG recordings and preprocessing

All participants underwent baseline EEG assessments, and iRBD patients had biannual EEG follow-up assessments. For the further analysis, we used the baseline EEG data and the most recent EEG data from the serial follow-up assessments for the iRBD patients. Scalp EEGs were recorded using two different equipment setups due to the equipment change in 2020.

Between 2014 and 2019, a total of 52 datasets were collected using an EEG recording device (Grass Technologies, USA) with 60 electrodes positioned according to the international 10-10 system. The data were recorded at a sampling rate of 400Hz, with the linked ear as the reference and the AFz electrode as the ground. To capture eye movement artifacts, two electrooculography (EOG) channels were positioned at the outer canthus of each eye.

Since 2020, 23 datasets were collected using an EEG recording device (Brain Products GmbH, Germany), with 64 electrodes positioned based on the international 10-10 system, and a sampling frequency of 500 Hz. The FCz electrode served as the reference, and the FPz electrode served as the ground. For both equipment settings, impedance of electrodes was kept below 10 kΩ during the recording.

Resting-state EEG data were collected for a total of 5 minutes while participants were in awake state. The eye-closed and eye-open conditions were alternated every 30 seconds, with 5 repetitions for each condition. The signals were filtered using a notch filter at 60Hz and a high pass filter at 0.5Hz. We selected 58 channels (excluding AFz, FPz, and FCz) that were common to both EEG recording devices. Subsequently, the signals were re-referenced to an average reference. For our analysis, only eye-closed resting EEG data were extracted and used.

To remove artifacts, we initially excluded segments that were severely contaminated by body movements through visual inspection. We then conducted independent component analysis and automatically removed components labeled as 'Eye' with a probability exceeding 90%.[19,20] Additionally, we manually rejected

other components that significantly affected the signal quality.

Finally, we extracted uncontaminated segments of 101 seconds from the data and resampled them at a frequency of 250 Hz. EEG data were preprocessed using EEGLAB v2021.0 in MATLAB R2020b (MathWorks, Natick, MA, USA).[21]

2.3. EEG data analysis

To achieve higher spatial resolution, we employed the source localization technique on the scalp EEG data. Source estimation was performed using the sLORETA method, implemented through Brainstorm version 3.23, which is executable within MATLAB.[22,23] We utilized a diagonal noise covariance matrix, and the current dipoles were constrained to be normal to cortex. This resulted in a source space consisting of 15002 vertices on the cortical surface. For visualization and further analysis to identify significant regions, we averaged the values of the 15002 vertices to 148 regions of interest defined by Destrieux atlas.[24]

We computed the power spectral density (PSD) using Welch's method in the source space. For this analysis, we used a 2-second window with 50% overlap, resulting in a frequency resolution of 0.5Hz for the power spectrum. To obtain relative PSD values for each source, we divided the PSD by the total power from 1Hz to 30Hz. Next, we calculated the relative band power values for each participant based on the conventional frequency bands, including delta (1-3.5Hz), theta (4-6.5Hz), alpha (7-12.5Hz), beta1 (13-19.5Hz), and beta2 (20-30Hz). Additionally, we evaluated dominant occipital frequency (DOF) within the range of 4-14Hz. The DOF was calculated by averaging the peak frequency values obtained from the seeds of all occipital scouts within the Destrieux atlas.

2.4. EEG spectro-spatial covariance pattern

To identify spectro-spatial covariance patterns related to phenoconversion, we applied SSM/PCA method to EEG data.[4] The

input data for the SSM/PCA method consisted of the relative power of each frequency band in source space. To derive the PD−RBD pattern and the DLB−RBD pattern, we utilized data from each disease group, along with age−, and sex− matched HC group data, in a 1:1 ratio. For the disease group, we used the most recent data collected after phenoconversion.

Following the SSM/PCA method, we obtained principal component (PC) and selected the top 5 PCs that explained the highest variance in the data. To obtain patterns that best discriminate the patients from control group, we performed logistic regression iteratively, using every possible combination of scores for the 5 PCs as independent variables, and the group as the dependent variable. The model with lowest Akaike Information Criterion (AIC) was selected to create disease patterns. Patterns were obtained by linear combinations of the selected PC patterns and were subsequently Z−transformed. This process resulted in PD−RBD and DLB−RBD patterns for each frequency band, producing a total of 10 patterns.

Since we did not have an independent prospective dataset of patients or a separate HC group, we applied the Leave−one−out cross−validation (LOOCV) method to validate our patterns.[25,26] In LOOCV, each subject from the group used for pattern generation was validated using a pattern derived from all other subjects (excluding the corresponding subject). This same pattern was also used to validate the subject' s baseline data. On the other hand, when validating subject from other groups, the pattern obtained from the entire set of subjects was used to calculate subject' s score. This approach allowed us to obtain the pattern expression scores that were independent from pattern derivation.[25]

For all participants, the individual pattern expression scores for each pattern were evaluated and normalized using Z−transform with respect to the HC group. The overall procedure for the derivation and validation of patterns is illustrated in Figure 1.

Figure 1. SSM/PCA procedure for EEG data

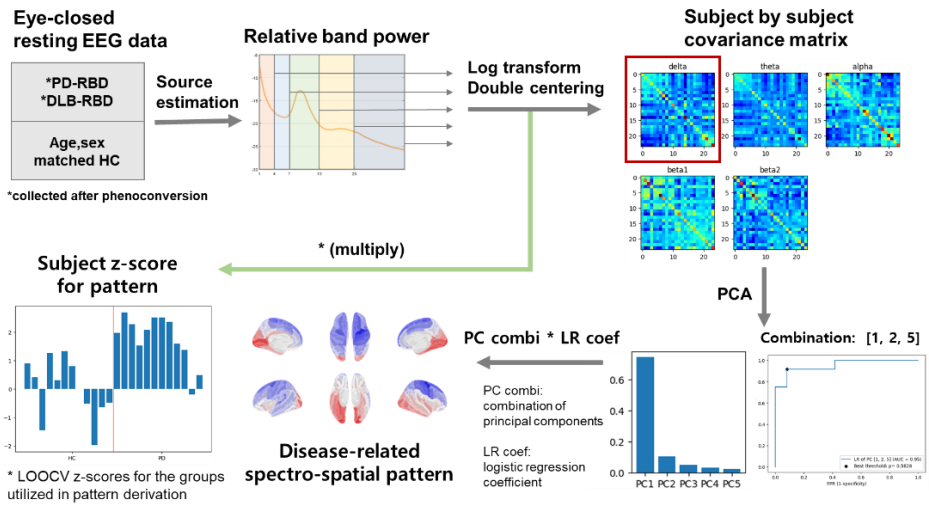

Abbreviations: SSM/PCA, Scaled Subprofile Model using principal component analysis. This figure illustrates the overall procedure of applying SSM/PCA to EEG data

2.5. Statistical analysis

Group differences in demographics and pattern expression z-scores were assessed using the Kruskal-Wallis test with Dunn's post-hoc test or Wilcoxon's rank-sum test for continuous variables, and Fisher's exact test for categorical variables. To evaluate the discriminative performance of the patterns, we calculated the area under the receiver operating characteristic (ROC) curve (AUC). The optimal cutoff for classification was determined using Youden's index. Correlations between clinical information and pattern expression were evaluated by partial Spearman's correlation, adjusting for age and sex. Similarly, for the correlation between DOF and pattern expression, the same method was used. A significance level of 0.05 was used to determine statistical significance. All statistical analyses were performed using Python 3.8.16 (Python Software Foundation, Wilmington, DE, USA) with the SciPy 1.10.1 and Pingouin 0.5.3.

Chapter 3. Results

3.1. Participant characteristics

In our study, a total of 47 participants were included, consisting of 35 patients with iRBD and 12 HC. Among the iRBD patients, 18 developed an overt α-synucleinopathy, with 12 developing PD (PD-RBD) and 6 developing DLB (DLB-RBD). Meanwhile, 17 patients did not phenoconvert throughout the follow-up period and were classified as iRBD nonconverters (iRBD-NC). One DLB-RBD subject had no baseline EEG data, and follow-up EEG data of 6 iRBD-NC subjects were not available. All other iRBD patients had both baseline and follow-up EEG data available for analysis.

Demographic characteristics are shown in Table 1. PD-RBD patients were younger than both DLB-RBD patients and iRBD-NC patients at both baseline and follow-up time points (Kruskal-Wallis test, p=0.0017 at baseline and p=0.0045 at follow-up). The cohort follow-up duration was defined from the date of iRBD diagnosis to the date of the last clinical visit, while the EEG follow-up duration was defined as the time from the baseline EEG examination to the follow-up EEG examination. No significant differences were observed between groups in terms of sex, cohort follow-up duration, and EEG follow-up duration.

For the cognitive and motor examinations, we used the data collected at the follow-up time point for the PD-RBD and DLB-RBD groups, whereas we utilized the data collected at the baseline time point for the iRBD-NC group. DLB-RBD patients had lower MoCA-K scores compared to PD-RBD, iRBD-NC patients, and HC (Kruskal-Wallis test, p=0.0019, Table 1). Additionally, MDS-UPDRS part III scores were higher in PD and DLB converters compared to iRBD-NC patients (Wilcoxon rank-sum test, p=0.00062, Table 1).

Table 1. Demographics

		PD-RBD (n=12)	DLB-RBD (n=6)	HC (n=12)	iRBD-NC (n=17)	P value
Baseline data	Age	66.8 (5.37) (57-71)	78.2 (3.77) (74-82) (n=5)	70.8 (5.39) (58-76)	73.2 (5.76) (59-82)	0.0017[a]
	Sex (m %)	58.3%	40.0% (n=5)	58.3%	58.8%	0.92
Follow-up data	Age	71.7 (6.05) (59-82)	80.2 (2.93) (76-84)		77.8 (4.87) (69-87) (n=11)	0.0045[b]
	Sex (m %)	58.3%	33.3%		63.6% (n=11)	0.56
Cohort follow up duration (year)		4.3 (1.69)	2.7 (1.10)		4.9 (2.48)	0.076
EEG follow up duration (year)		4.8 (2.25)	2.5 (1.20) (n=5)		3.6 (1.86) (n=11)	0.15
Follow up data for PD-RBD, DLB-RBD, baseline data for iRBD-NC						
MoCA-K		26.0 (3.67) (n=9)	16.5 (5.01) (n=6)	26.8 (1.40)	24.8 (3.63) (n=17)	0.0019[c]
MDS-UPDRS part III		9.1 (4.94) (n=9)	17.4 (10.96) (n=4)		2.5 (3.63) (n=14)	0.00062*

Abbreviations: PD-RBD, iRBD patients who converted to PD; DLB-RBD, iRBD patients who converted to DLB; HC, healthy controls; iRBD-NC, iRBD nonconverters; MoCA-K, Korean version of the Montreal Cognitive Assessment; MDS-UPDRS, Movement Disorder Society-Sponsored Revision of the Unified Parkinson's Disease Rating Scale.

a PD-RBD < DLB-RBD (p=0.0025), PD-RBD < iRBD-NC (p=0.019)

b PD-RBD < DLB-RBD (p=0.0070), PD-RBD <iRBD-NC (p=0.037)

c DLB-RBD < PD-RBD (p=0.0052), DLB-RBD < iRBD-NC (p=0.023), DLB-RBD < HC (p=0.0016)

* Wilcoxon rank sum test (PD-RBD, DLB-RBD vs iRBD-NC) due to number of DLB-RBD patients <5

3.2. PD-RBD related EEG spectro-spatial covariance pattern

For each of the five frequency bands, we derived the PD-RBD related EEG spectro-spatial covariance pattern using data from 12 PD-RBD patients and 12 age-, and sex- matched HC (Figure 2). As mentioned in the method section, PD-RBD patients' follow-up data after phenoconversion were utilized. Detailed descriptions on derived patterns are provided in Table 2. Among the five patterns, the delta pattern and alpha pattern showed the best discrimination between PD-RBD and HC (AUC=0.8522 and 0.9097 for PD-RBD delta pattern, PD-RBD alpha pattern, respectively). Regions that significantly positively and negatively contributed to each pattern are presented in Table 3.

The PD-RBD delta pattern was characterized by relatively increased power in the left and right occipital poles, while showing relatively decreased power in the right precentral gyrus and superior part of the precentral sulcus (absolute z-scores > 2.0, Figure 3). We evaluated the differences in z-scores for the PD-RBD delta pattern between HC, PD-RBD, DLB-RBD, and iRBD-NC groups. For iRBD-NC group, we used z-scores obtained from baseline data. The pattern expression z-scores of the PD-RBD group were higher than those of the iRBD-NC group and HC (post-hoc p= 0.038 and 0.011, respectively). DLB-RBD patients also have higher z-scores for the pattern than the iRBD-NC group and HC (post-hoc p= 0.011 and 0.0028, respectively).

The PD-RBD alpha pattern exhibited relatively increased power in the right fronto-marginal gyrus and sulcus, transverse frontopolar gyri and sulci, postcentral gyrus, and precentral gyrus (absolute z-scores > 2.0, Figure 3). The pattern expression z-scores of the PD-RBD group were higher than those of the iRBD-NC group and HC (post-hoc p=0.0091 and 0.00078, respectively), and the DLB-RBD group also had higher z-scores than the iRBD-NC group and HC (post-hoc p= 0.014 and 0.0022, respectively).

Figure 2. PD−RBD related EEG spectro−spatial covariance pattern

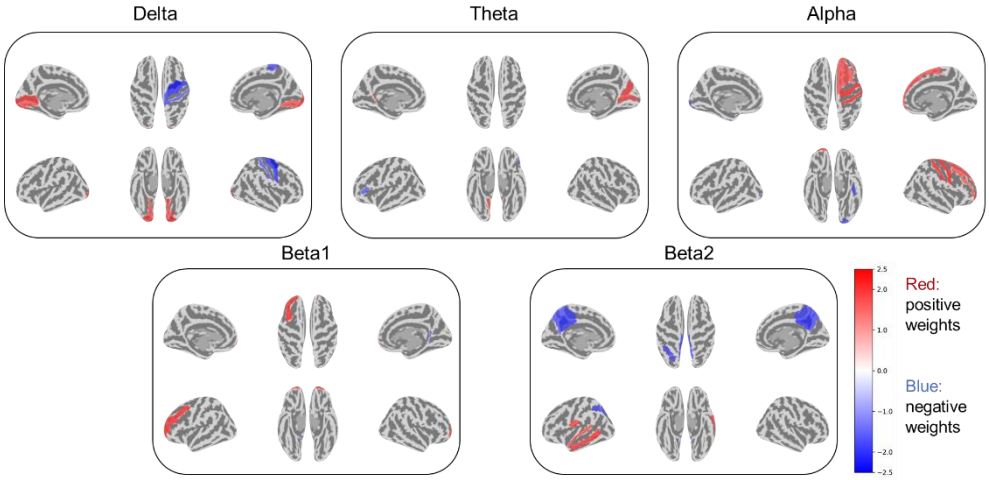

Abbreviations: PD−RBD, iRBD patients who converted to PD.

This figure presents the PD−RBD pattern for all frequency bands. 15002 voxels were averaged to 148 regions of interest (ROIs) defined by Destrieux atlas. This figure was displayed in neurological convention. Red colors mean regions with relative increased power, and blue colors mean regions with relative decreased power. Only the regions with |z| >1.7507 (96%) were shown.

Table 2. PD−RBD related EEG spectro−spatial covariance pattern

Frequency band	Combinations of PCs	explained variance	AUC	P value
Delta	1, 2, 5	0.87	0.8522	0.00033
Theta	1, 2	0.85	0.6458	0.015
Alpha	1, 2, 4, 5	0.85	0.9097	$4.74*10^{-5}$
Beta1	1, 5	0.77	0.8333	0.00049
Beta2	1, 2, 5	0.86	0.8333	0.00034

Abbreviations: AUC, area under the receiver operating characteristic curve.
P value: p value of Wilcoxon rank−sum test

Table 3. Significant brain regions in PD−RBD related spectro−spatial covariance pattern

Frequency band	Positive components	Z	Negative components	Z
delta	Lingual gyrus L	1.79906	Paracentral lobule and sulcus R	−1.8801
	Lingual gyrus R	1.87291	Postcentral gyrus R	−1.7914
	Occipital pole L	**2.77505**	Precentral gyrus R	**−2.2092**
	Occipital pole R	**2.16212**	Superior part of the precentral sulcus R	**−2.4503**
	Calcarine sulcus L	1.974		
	Posterior transverse collateral sulcus L	1.97541		
theta	Posterior−ventral part of the cingulate gyrus L	1.86371	Triangular part of the inferior frontal gyrus L	−1.7767
	Calcarine sulcus R	1.76388		
	Parieto−occipital sulcus R	1.82659		
alpha	**Fronto−marginal gyrus and sulcus R**	**2.0888**	Occipital pole L	−1.9953
	Transverse frontopolar gyri and sulci R	**2.01682**	Anterior transverse collateral sulcus L	−1.779
	Middle frontal gyrus R	1.79839		
	Superior frontal gyrus R	1.83624		
	Postcentral gyrus R	**2.35152**		
	Precentral gyrus L	1.70167		
	Precentral gyrus R	**2.42486**		
	Superior frontal sulcus R	1.79227		
beta1	Fronto−marginal gyrus and sulcus L	1.9462	Posterior−ventral part of the cingulate gyrus R	−1.8651
	Fronto−marginal gyrus and sulcus R	1.78393		
	Transverse frontopolar gyri and sulci L	**2.0144**		
	Transverse frontopolar gyri and sulci R	1.96082		
	Middle frontal gyrus L	**2.2989**		
	Middle frontal sulcus L	1.95554		
beta2	**Subcentral gyrus and sulci L**	**2.02836**	**Posterior−dorsal part of the cingulate gyrus L**	**−2.2026**
	Lateral aspect of the superior temporal gyrus L	1.94743	**Posterior−dorsal part of the cingulate gyrus R**	**−2.2052**
	Middle temporal gyrus L	**2.22973**	Precuneus L	−1.8451

	Transverse temporal sulcus L	1.79819	Precuneus R	−1.8776
			Marginal branch of the cingulate sulcus L	−1.9727
			Marginal branch of the cingulate sulcus R	−1.8792
			Intraparietal sulcus and transverse parietal sulci L	−1.7786
			Subparietal sulcus L	**−2.1814**
			Subparietal sulcus R	**−2.1979**

Abbreviations: L, left; R, right.
Only regions with an average z−score greater than 1.7507 (96%) were indicated.
Regions with z−scores greater than 2.0 were indicated in bold.

Figure 3. PD-RBD pattern and pattern expression values

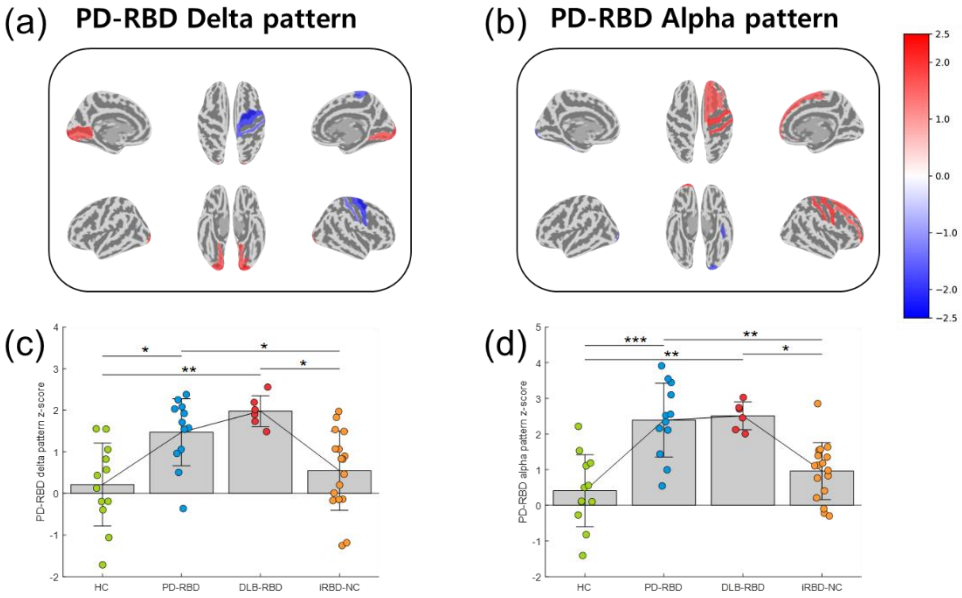

(a) PD-RBD delta pattern (b) PD-RBD alpha pattern

(c) PD-RBD delta pattern expression (d) PD-RBD alpha pattern expression

Abbreviations: HC, healthy controls; PD-RBD, iRBD patients who converted to PD; DLB-RBD, iRBD patients who converted to DLB; iRBD-NC, iRBD nonconverters.

The figure illustrates two PD-RBD patterns that effectively distinguish PD-RBD patients from HC. The distribution of subject z-scores for each group corresponding to the respective patterns is also shown. 15002 voxels were averaged to 148 regions of interest (ROIs) defined by Destrieux atlas. This figure was displayed in neurological convention. Red colors mean regions with relative increased power, and blue colors mean regions with relative decreased power. Only the regions with $|z| > 1.7507$ (96%) were shown. P values of post-hoc Dunn's test were calculated to compare group differences (*$p<0.05$, **$p<0.01$, ***$p<0.001$)

3.3. DLB-RBD related EEG spectro-spatial covariance pattern

The DLB-RBD related EEG spectro-spatial covariance pattern was derived using the same procedure as the PD-RBD pattern (Figure 4). Data from 6 DLB-RBD patients and 6 age- and sex-matched HC (age: 74.0±2.10, male %: 33.3%) were used for pattern derivation, and the results for all five patterns were presented in Table 4. For the DLB-RBD related pattern, the delta, alpha, and beta1 patterns demonstrated the best discrimination between DLB-RBD patients and HC (AUC = 0.9306 for delta, alpha, and beta1 patterns). Significant regions for each pattern were listed in Table 5.

The DLB-RBD delta pattern was characterized by relatively increased power in the left posterior-ventral part of the cingulate gyrus and the occipital pole, while showing relatively decreased power in the left middle frontal gyrus and superior frontal sulcus (absolute z-scores > 2.0, Figure 5). DLB-RBD patients exhibited higher z-scores for the delta pattern compared to the iRBD-NC group and HC (post-hoc p= 0.023 and 0.014, respectively).

The DLB-RBD alpha pattern exhibited relatively increased power in the left and right precentral gyrus, postcentral gyrus, and the right superior part of the precentral sulcus (absolute z-scores > 2.0, Figure 5). DLB-RBD patients had higher z-scores for the alpha pattern compared to the iRBD-NC group and HC (post-hoc p= 0.025 and 0.0045, respectively), and the z-scores of PD-RBD patients were also higher than those of the iRBD-NC group and HC (post-hoc p= 0.019 and 0.0019, respectively).

The DLB-RBD beta1 pattern showed positive weights in the right transverse frontopolar gyri and sulci, middle frontal gyrus, and middle frontal sulcus (absolute z-scores > 2.0, Figure 5). DLB-RBD patients had higher z-scores for the beta1 pattern compared to the iRBD-NC group and HC (post-hoc p= 0.012 and 0.016, respectively), and the z-scores of PD-RBD patients were also higher than those of the iRBD-NC group and HC (post-hoc p= 0.020 and 0.028, respectively).

Figure 4. DLB-RBD related EEG spectro-spatial covariance pattern

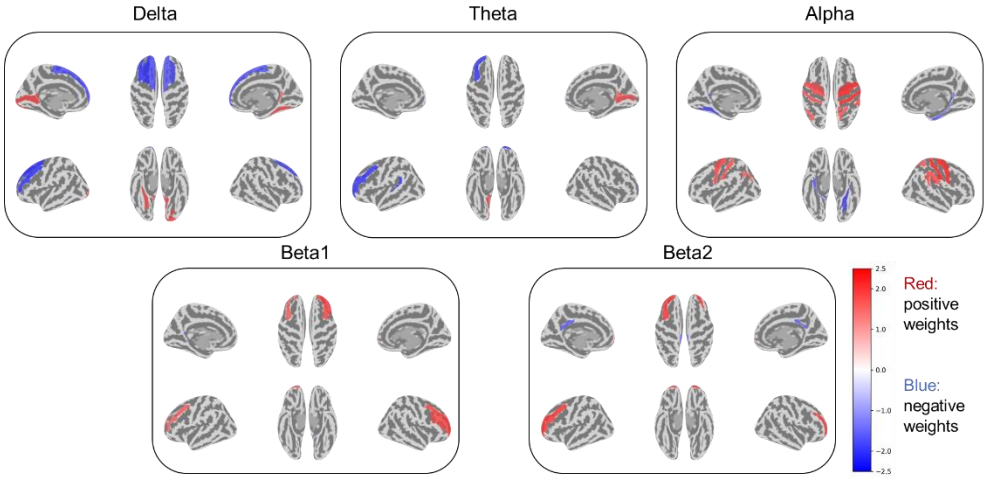

Abbreviations: DLB-RBD, iRBD patients who converted to DLB.

This figure presents the DLB-RBD pattern for all freuquency bands. 15002 voxels were averaged to 148 regions of interest (ROIs) defined by Destrieux atlas. This figure was displayed in neurological convention. Red colors mean regions with relative increased power, and blue colors mean regions with relative decreased power. Only the regions with |z| >1.7507 (96%) were shown.

Table 4. DLB−RBD related EEG spectro−spatial covariance pattern

Frequency band	Combinations of PCs	explained variance	AUC	P value
Delta	1, 2	0.82	0.9306	0.0027
Theta	1, 2, 4, 5	0.94	0.8194	0.021
Alpha	1, 2	0.67	0.9306	0.00018
Beta1	1, 2	0.93	0.9306	0.00088
Beta2	1, 2, 4, 5	0.94	0.8750	0.0038

Abbreviations: AUC, area under the receiver operating characteristic curve.
P value: p value of Wilcoxon rank−sum test

Table 5. Significant brain regions in DLB−RBD related spectro−spatial covariance pattern

Frequency band	Positive regions	Z	Negative regions	Z
delta	**Posterior−ventral part of the cingulate gyrus L**	**2.10903**	Transverse frontopolar gyri and sulci R	−1.7579
	Posterior−ventral part of the cingulate gyrus R	1.87917	**Middle frontal gyrus L**	**−2.3328**
	Occipital pole L	**2.05694**	Superior frontal gyrus L	−1.9611
	Calcarine sulcus L	1.90939	Superior frontal gyrus R	−1.8779
	Posterior transverse collateral sulcus L	1.94669	**Superior frontal sulcus L**	**−2.1799**
	Collateral sulcus and lingual sulcus R	1.78477	Superior frontal sulcus R	−1.8582
theta	Posterior−ventral part of the cingulate gyrus R	1.84967	Fronto−marginal gyrus and sulcus L	−1.9728
	Calcarine sulcus R	1.76605	**Transverse frontopolar gyri and sulci L**	**−2.0434**
			Transverse frontopolar gyri and sulci R	**−2.0736**
			Middle frontal gyrus L	**−2.2757**
			Temporal plane of the superior temporal gyrus L	−1.9935
			Middle frontal sulcus L	−1.908
alpha	Angular gyrus L	1.83144	Posterior−ventral part of the cingulate gyrus L	−1.7937
	Supramarginal gyrus R	1.96957	Posterior−ventral part of the cingulate gyrus R	−1.8918
	Superior parietal lobule R	1.85947	Parahippocampal gyrus R	−1.8236
	Postcentral gyrus L	**2.04817**	Collateral sulcus and lingual sulcus L	−1.8103
	Postcentral gyrus R	**2.73724**		
	Precentral gyrus L	**2.07828**		
	Precentral gyrus R	**2.65041**		
	Sulcus intermedius primus R	1.77018		
	Superior part of the precentral sulcus L	1.83549		
	Superior part of the precentral sulcus R	**2.07628**		
beta1	Fronto−marginal gyrus and sulcus R	1.84943	Posterior−ventral part of the cingulate gyrus L	−1.8378
	Transverse frontopolar gyri and sulci R	**2.09625**		

	Middle frontal gyrus L	1.85019		
	Middle frontal gyrus R	**2.07357**		
	Inferior frontal sulcus R	1.87641		
	Middle frontal sulcus R	**2.03476**		
beta2	**Fronto−marginal gyrus and sulcus L**	**2.07683**	Posterior−dorsal part of the cingulate gyrus L	−1.8545
	Fronto−marginal gyrus and sulcus R	1.8827	Posterior−dorsal part of the cingulate gyrus R	−1.7941
	Transverse frontopolar gyri and sulci L	**2.08899**		
	Transverse frontopolar gyri and sulci R	**2.07202**		
	Middle frontal gyrus L	**2.23795**		
	Middle frontal sulcus L	**2.05368**		
	Middle frontal sulcus R	1.83836		

Only regions with an average z−score less than −1.7507 (96%) were indicated
Regions with z−scores less than −2.0 were indicated in bold.

Figure 5. DLB-RBD pattern and pattern expression values

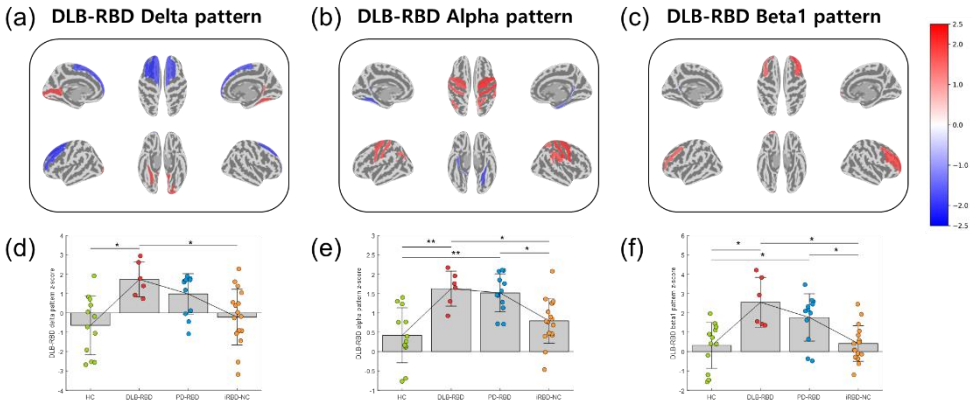

(a) DLB-RBD delta pattern (b) DLB-RBD alpha pattern
(c) DLB-RBD beta1 pattern (d) DLB-RBD delta pattern expression
(e) DLB-RBD alpha pattern expression (f) DLB-RBD beta1 pattern expression
Abbreviations: HC, healthy controls; DLB-RBD, iRBD patients who converted to DLB; PD-RBD, iRBD patients who converted to PD; iRBD-NC, iRBD nonconverters.
The figure illustrates two DLB-RBD patterns that effectively distinguish DLB-RBD patients from HC. The distribution of subject z-scores for each group corresponding to the respective patterns is also shown. 15002 voxels were averaged to 148 regions of interest (ROIs) defined by Destrieux atlas. This figure was displayed in neurological convention. Red colors mean regions with relative increased power, and blue colors mean regions with relative decreased power. Only the regions with $|z| > 1.7507$ (96%) were shown. P values of post-hoc Dunn's test were calculated to compare group differences (*$p<0.05$, **$p<0.01$, ***$p<0.001$)

3.4. Clustering by combined EEG spectro-spatial pattern

In order to identify EEG spectro-spatial patterns as useful biomarkers for predicting early phenoconversion and also its subtype, we combined two of the patterns derived earlier to create a 2D plane, which we termed the "Combined pattern space". This allowed us to visualize the pattern expression of each individual in a 2D plane. The analysis of the combined pattern space is divided into two steps: first, creating a space that reflects the characteristics of the diseases, and second, applying this space to the baseline data for longitudinal analysis. In this section, we focused on the first step of creating the space, while longitudinal analysis will be discussed in a later section.

To create the combined pattern space, we set the x-axis as the z-score for the pattern that best discriminated the iRBD converters (PD-RBD, DLB-RBD) from iRBD nonconverters, which may represent a biomarker for early phenoconversion of α-synucleinopathies. Similarly, the y-axis was set as the z-score for the pattern that best distinguished the PD-RBD and DLB-RBD groups, which may represent a biomarker for subtypes of phenoconversion of α-synucleinopathies. Specifically, we selected the PD-RBD alpha pattern z-score (AUC= 0.8856) for the x-axis and the DLB-RBD theta pattern z-score (AUC= 0.8611) for the y-axis. The decision boundaries for the two axes were established using Youden's index from the ROC curve (z= 2.005 for the x-axis and z=1.6563 for the y-axis). Combined pattern space was represented in Figure 6.

In addition, we found that the DLB-RBD theta pattern had a significant negative correlation with the DOF, which is known to reflect cognitive function (rho=-0.6147, p= 0.00014). Thus, the x-axis represents the overall conversion status, while the y-axis reflects the severity of cognitive impairment.

By applying the decision boundaries, we were able to divide the individuals into four groups, each characterized by the following features: Group 1: dementia and α-synucleinopathy, Group 2: PD

and α−synucleinopathy, Group 3: normal state, and Group 4: mild cognitive impairment (MCI) or aging. This combined space will be used in the further analysis.

Figure 6. Clustering by combined EEG spectro-spatial pattern

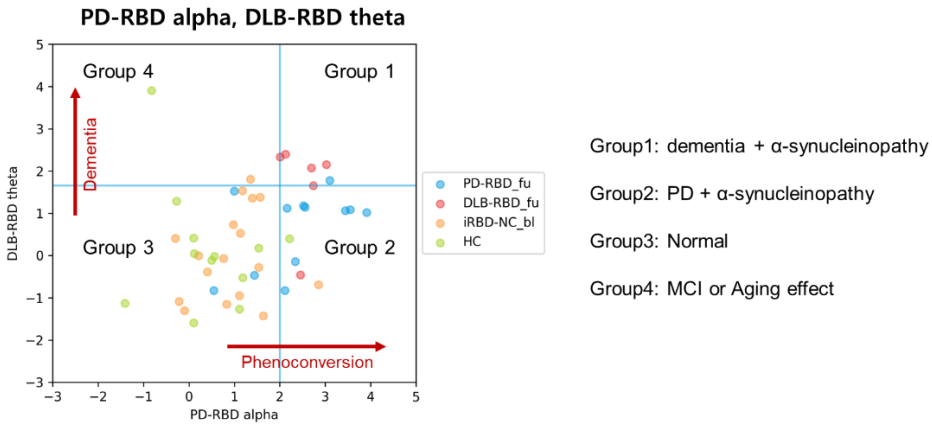

Abbreviations: PD-RBD_fu, follow-up data of iRBD patients who converted to PD; DLB-RBD_fu, follow-up data of iRBD patients who converted to DLB; iRBD-NC_bl, baseline data of iRBD nonconverters; HC, data of healthy controls; MCI, mild cognitive impairment.

This figure illustrates the combined pattern space, created by combining two patterns. PD-RBD alpha pattern expression on the x-axis, reflecting early phenoconversion, and DLB-RBD theta pattern expression on the y-axis, reflecting phenoconversion subtype. The space is divided into four groups, and the characteristics of each group are described on the right side. Data points for each group are represented by different colors (PD-RBD_fu: blue, DLB-RBD_fu: red, iRBD-NC_bl: yellow, HC: green)

3.5. Correlation between patterns and clinical characteristics

To explore the relevance of pattern expression to clinical characteristics, we conducted correlation analysis. Using partial Spearman' s correlation, adjusted for age and sex, we analyzed all subjects with available MDS-UPDRS part III scores (n= 27) and MoCA-K scores (n= 44). Firstly, we found a positive correlation between the MDS-UPDRS part III scores, which reflect motor symptom severity, and the z-scores for the PD-RBD delta, theta, alpha, and beta1 patterns (rho= 0.688, p=0.00014 for PD-RBD delta pattern; rho= 0.469, p= 0.018 for PD-RBD theta pattern; rho= 0.582, p= 0.0022 for PD-RBD alpha pattern; and rho= 0.415, p= 0.039 for PD-RBD beta1 pattern). The strongest correlation was observed with the PD-RBD delta pattern (Figure 7(a)).

Additionally, the MDS-UDPRS part III scores were positively correlated with the z-scores for the DLB-RBD delta and beta1 pattern (rho= 0.539, p= 0.0055 for DLB-RBD delta pattern; rho= 0.430, p=0.032 for DLB-RBD beta1 pattern), although the correlations were weaker compared to the PD-RBD delta pattern (Figure 7(b)).

On the other hand, no significant correlation was found between MoCA-K scores and any of the pattern expression values.

Figure 7. Correlation between pattern expression and MDS−UPDRS part III

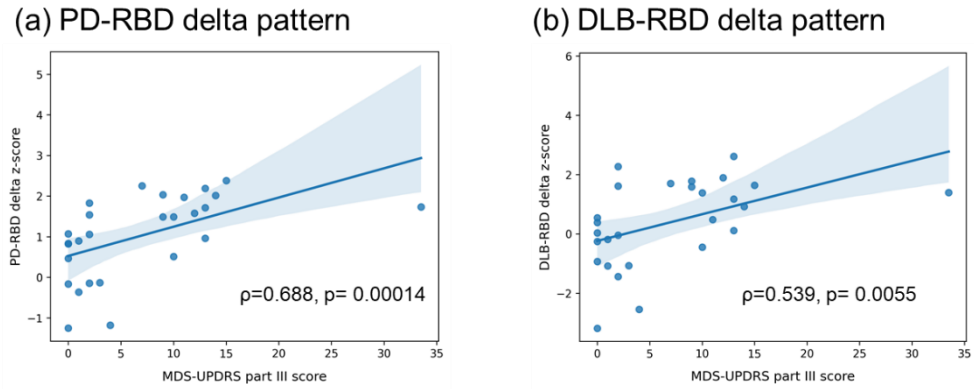

Abbreviations: MDS−UPDRS, Movement Disorder Society−Sponsored Revision of the Unified Parkinson' s Disease Rating Scale; PD−RBD, iRBD patients who converted to PD; DLB−RBD, iRBD patients who converted to DLB.

(a) MDS−UPDRS part III score and PD−RBD delta pattern expression

(b) MDS−UPDRS part III score and DLB−RBD delta pattern expression

ρ , p: Partial Spearman' s correlation coefficient and p value, adjusted for age and sex.

3.6. Pattern expression level at the baseline

We investigated whether there were differences in pattern expression between iRBD converters (PD−RBD, DLB−RBD) and nonconverters at baseline. For both PD−RBD and DLB−RBD patterns, the beta2 patterns demonstrated the modest differentiation between iRBD converters and nonconverters (AUC= 0.7751, rank−sum test p= 0.0062 for PD−RBD beta2 pattern and DLB−RBD beta2 pattern, Figure 8).

Figure 8. Pattern expression at the baseline

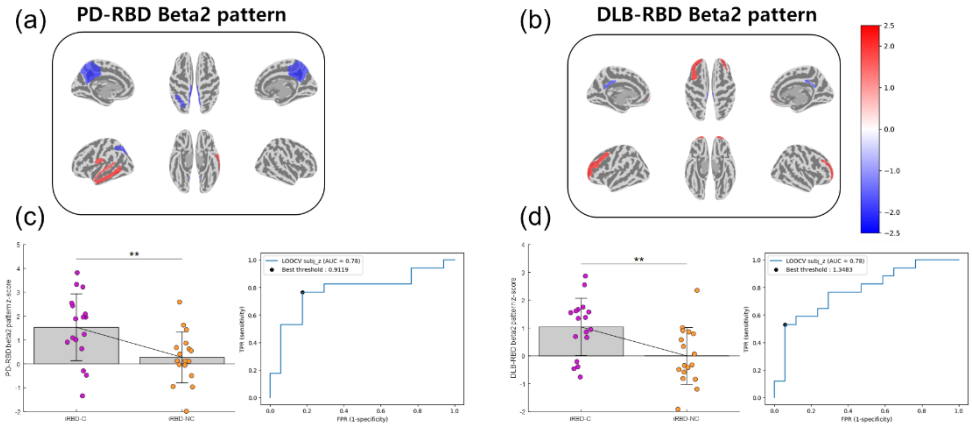

Abbreviations: PD−RBD, iRBD patients who converted to PD; DLB−RBD, iRBD patients who converted to DLB; iRBD−C, iRBD converters; iRBD−NC, iRBD nonconverters; LOOCV, Leave−one−out cross−validation; FPR, false positive rate; TPR, true positive rate; ROC, receiver operating characteristic; AUC, area under the receiver operating characteristic curve.

(a) PD−RBD beta2 pattern (b) DLB−RBD beta2 pattern

(c) PD−RBD beta2 pattern expression and ROC curve to discriminate iRBD converters from iRBD nonconverters at baseline

(d) DLB−RBD beta2 pattern expression and ROC curve to discriminate iRBD converters from iRBD nonconverters at baseline

The figure illustrates two patterns that effectively distinguish iRBD converters from iRBD nonconverters at baseline. The distribution of subject z−scores and ROC curves to discriminate two groups are also shown. 15002 voxels were averaged to 148 regions of interest (ROIs) defined by Destrieux atlas. This figure was displayed in neurological convention. Red colors mean regions with relative increased power, and blue colors mean regions with relative decreased power. Only the regions with $|z| > 1.7507$ (96%) were shown. P values of Wilcoxon rank−sum were calculated to compare group differences (*$p<0.05$, **$p<0.01$, ***$p<0.001$)

3.7. Longitudinal trajectory in combined pattern space

Finally, we projected the baseline and follow-up data of all subjects onto the previously derived combined pattern space to visualize the changes over time. At baseline, most subjects were located in Group 3, but after the follow-up period, there was a noticeable shift of data points towards the right side of the plane.

We represented individual longitudinal trajectories separately for each group (Figure 9). In the PD-RBD patients, most data points showed a horizontal rightward shift in their individual trajectories over time, moving from Group 3 to Group 2. For DLB-RBD patients, most data points moved to the upper right, transitioning from Group 3 to Group 1. For iRBD nonconverters, most data points did not cross the boundary after follow-up, but they exhibited progression in the rightward direction or the upper-right direction.

Figure 9. Longitudinal trajectory of combined spatial pattern expression

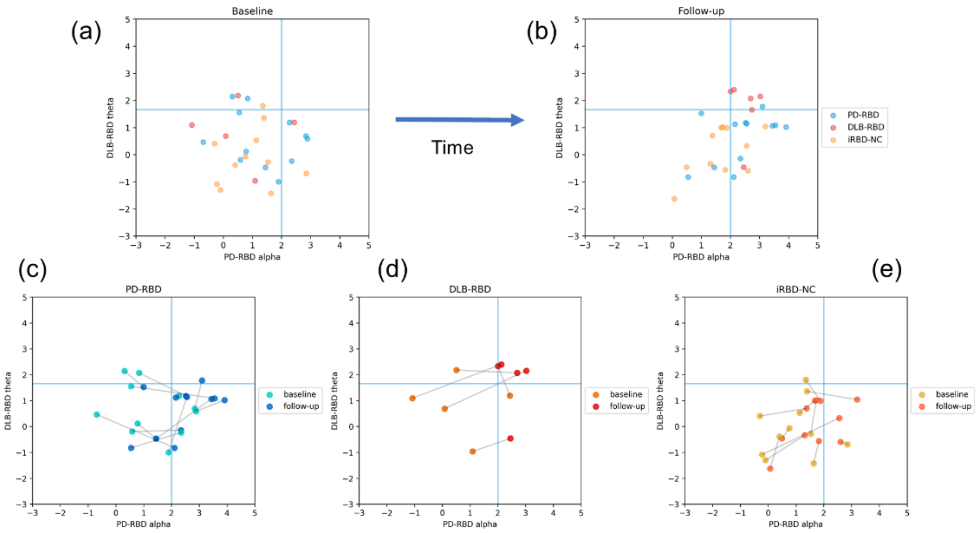

Abbreviations: PD−RBD, iRBD patients who converted to PD; DLB−RBD, iRBD patients who converted to DLB; iRBD−NC, iRBD nonconverters.

(a) all subjects at baseline (b) all subjects at follow−up

(c) Longitudinal trajectory of PD−RBD subjects

(d) Longitudinal trajectory of DLB−RBD subjects

(e) Longitudinal trajectory of iRBD−NC subjects

This figure illustrates the longitudinal trajectory in the combined pattern space. (a) and (b) show the positions of all subjects at baseline and follow−up in the combined pattern space, respectively. (c), (d), and (e) display the individual trajectories of PD−RBD, DLB−RBD, and iRBD−NC subjects, respectively. Baseline positions are represented by lighter dots, while follow−up positions are indicated by darker dots.

Chapter 4. Discussion

In this study, our aim was to identify EEG spectro-spatial covariance patterns associated with phenoconversion in iRBD patients and investigate their clinical relevance and longitudinal trajectories. Notably, the PD-RBD and DLB-RBD related EEG patterns exhibited spatial features that were consistent with previously identified brain metabolic covariance patterns associated with PD and DLB. Furthermore, PD-RBD and DLB-RBD patients showed similar spatial characteristics in their EEG patterns, with increased expression in patterns derived from each other. Delta and alpha patterns appeared to effectively reflect the overall progression of α-synucleinopathies. We created a combined pattern space by combining pattern expression scores, which effectively distinguished groups based on their spatial distributions. However, at the baseline, pattern expression scores did not clearly differentiate iRBD converters from nonconverters. Longitudinal tracking of PD-RBD, DLB-RBD and iRBD-NC groups revealed that individuals gradually shifted towards the right or upper-right region of the plane. This suggests that the expression of EEG spectro-spatial covariance patterns might initiate at a later stage compared to brain metabolism patterns in iRBD patients. As a result, the complementary use of patterns derived from both modalities may prove valuable in assessing the current status and estimating the risk of phenoconversion and its subtypes in iRBD patients.

Comparison with the previously identified brain metabolic patterns

Our results demonstrated that both PD-RBD and DLB-RBD delta and alpha patterns effectively distinguished PD patients and DLB patients from the HC group. Previous studies have reported brain metabolic patterns related to PD, DLB, and RBD using [^{18}F]FDG-PET imaging data. The PD related metabolic pattern (PDRP) showed relatively hypermetabolism in putamen, thalamus, globus pallidus, cerebellum, and pons, and relatively hypometabolism in the

occipitoparietal cortex.[5,27] Similarly, the DLB related metabolic pattern (DLBRP) exhibited relative metabolic increases in the pallidum, putamen, amygdala, hippocampus, parahippocampi, cerebellum, and pons, along with decreases in the occipital, parietal and temporal cortex, and precuneus.[7,28] As for RBD related metabolic pattern (RBDRP), they differed among research groups because RBD is a transitional state. However, these patterns commonly exhibit negative contributions from the occipital, parietal, and temporal regions, while being positively contributed to by the premotor cortex, frontal cortex, and hippocampus.[8,29,30] And pattern derived from de novo PD patients with a history of RBD before developing parkinsonism (dnPDRBD) shares characteristics of both PDRP and RBDRP.[6] The dnPDRBD related metabolic pattern (dnPDRBDRP) exhibited distinguishing features, such as relative hypometabolism in the lingual gyrus and hypermetabolism in the premotor cortex. Notably, dnPDRBDRP was reported to have better predictability for future phenoconversion in iRBD patients compared to PDRP. Our PD-RBD related spectro-spatial pattern and the dnPDRBDRP were derived from patient groups with almost identical characteristics, enabling a direct comparison between them.

We derived PD-RBD and DLB-RBD delta patterns, both of which showed common positive contributions from the occipital cortex. Previous studies have shown that the occipital cortex, including the lingual gyrus, showed hypometabolism in PD, RBD, and DLB. Considering that increased low-frequency power in the occipital region has been linked to cognitive impair or functional abnormalities in neurological conditions,[11,31,32] relative hypometabolism in occipital cortex could potentially be reflected as increased delta and theta band power in occipital cortex.

In our results, PD-RBD alpha pattern was characterized by increased power in the right frontal and central regions, while the DLB-RBD alpha pattern showed increased power in the precentral and postcentral gyrus. Some studies reported relative hypermetabolism in sensorimotor cortex, or motor cortex in PD, idiopathic RBD, and DLB related metabolic patterns.[27–30,33] And one

MEG study suggested that increased low alpha power (8−10Hz) in centroparietal region of de novo PD patients might be linked to cognitive impairments, particularly a pathologically elevated level of attention.[14] The interpretation of increased centroparietal alpha power requires further investigation.

Comparison between PD−RBD and DLB−RBD patterns

There was a significant overlap between PD−RBD and DLB−RBD patterns. Moreover, both groups of patients exhibited high pattern expression scores for each other' s pattern, suggesting a common underlying pathology, which is α−synucleinopathy. This finding is consistent with the considerable similarities observed between PD and DLB related brain metabolic patterns in their spatial features.[7,33] However, there were slight differences in the specific locations where the PD−RBD and DLB−RBD patterns contributed significantly. In the delta band, the DLB−RBD pattern showed a negative association in the frontal region. The PD−RBD pattern, on the other hand, displayed a relative increase in alpha power in the right frontal and central region, while the DLB−RBD pattern showed a relative increase in alpha power in the precentral and postcentral gyrus, slightly posterior to the frontal region.

Combined pattern space

We successfully divided the groups by combining two of pattern expression scores. The use of PD−RBD alpha pattern as the x−axis appeared to effectively reflect α −synucleinopathies, considering its positive correlation with MDS−UPDRS part III scores and its ability to discriminate between iRBD converters and nonconverters. On the other hand, the use of DLB−RBD theta pattern as the y−axis effectively distinguished DLB from PD. It was observed that subjects with low DOF tended to have higher theta scores regardless of the group. The shift of dominant occipital rhythm toward lower frequencies has been associated with cognitive deterioration in several neurodegenerative disorders.[11,12,34,35] Indeed, our DLB−RBD theta pattern exhibited relative increased power in posterior regions,

which might be influenced by the transition of occipital alpha rhythm into the theta band frequency range or by theta oscillation itself. In an MEG study, posterior delta and theta power were increased in mild cognitive impairment group than the cognitive normal group, and researchers suggested that increased low-frequency oscillations are related to general cognitive decline and hippocampal atrophy.[36] Thus, the DLB-RBD theta pattern can be considered to reflect overall cognitive functioning rather than specific pathology.

When tracking the longitudinal trajectory of the iRBD-NC, PD-RBD, and DLB-RBD groups in the combined pattern space, we observed changes in pattern expression over time for all three groups. This indicates an elevation in alpha pattern expression as the disease progresses. The DLB-RBD group' s upward shift suggests that cognitive deterioration may occur more prominently and progress at a faster rate. Furthermore, the longitudinal tracking of iRBD nonconverters revealed that the majority of them remained in Group 3 (normal state) even after mean 3.6 years of follow-up. However, individuals who are close to or cross the boundary may require special concern and close monitoring. The combined pattern space offers a promising approach for quantitative risk assessment of phenoconversion and its subtypes in iRBD patients.

Utility as a biomarker

Previous studies have demonstrated that brain metabolic covariance patterns associated with PD and DLB could predict future conversion at the baseline. For instance, one study used a pattern derived from dnPDRBD, and another study employed phenoconversion-related pattern in iRBD to predict the risk of phenoconversion in iRBD patients.[6,37] Additionally, a DLB-related cortical thickness pattern obtained from magnetic resonance imaging (MRI) was able to predict the dementia-first phenoconversion within 4 years from the baseline.[9] These findings suggest that brain metabolic or structural covariance patterns hold promise as biomarkers for predicting phenoconversion in iRBD patients.

In our study, we did not clearly discriminate iRBD converters

from nonconverters at the baseline using EEG spectro-spatial covariance patterns. While this may imply limitations in using EEG spectro-spatial covariance pattern as a biomarker for predicting phenoconversion, it also suggests that EEG may capture different aspects of phenoconversion-related changes compared to brain metabolism or structural changes. The lack of clear distinction at baseline and the observed increase in pattern expression values during follow-up indicate that EEG changes may not manifest clearly in the early stages of neurodegeneration. It could be hypothesized that pattern expression values may exhibit a nonlinear increase shortly before α-synucleinopathies become overt. Compensatory mechanisms are known to operate in EEG, as shown in a preclinical Alzheimer's disease study where PSD delta power followed a U shaped curve depending on the amyloid burden in the presence of neurodegeneration.[38] Moreover, our previous study reported compensatory mechanisms associated with cognitive impairment in iRBD patients.[39]

Hence, in iRBD patients, EEG may exhibit a compensatory mechanism to maintain normal functioning until a certain threshold is surpassed (close to phenoconversion), at which point the compensation collapses, and the EEG patterns undergo a rapid change. Thus, while our EEG spectro-spatial patterns may not serve as strong predictors for phenoconversion in the early stages of iRBD, the combined pattern space would offer potentially useful information about the risk of phenoconversion in the near future.

EEG spectro-spatial covariance pattern

In this study, we applied SSM/PCA method to EEG data. To maximize the advantage of the simplicity of EEG recording, we utilized EEG data in a resting state without performing any tasks. Previous studies have suggested that resting EEG alone can serve as a valuable biomarker for assessing disease status and cognitive function.[13,38,40,41] In our results, the pattern expression scores for delta and alpha patterns were significantly different between converters and nonconverters. This indicates that resting state EEG

provides sufficient information about disease status.

The SSM/PCA method offers several advantages, including the ability to visualize disease-specific spatial covariance patterns and quantify individual scores for these patterns. As mentioned earlier, while EEG slowing phenomenon in PD, DLB, and iRBD has been reported in many studies, individual-level evaluation of EEG characteristics to assess disease severity has been limited. With this approach, we presented disease-related spatial characteristics for each frequency band as a single figure. Furthermore, with only 5 minutes of EEG data, we were able to quantify phenoconversion risk using several scores at the individual level. Therefore, the EEG spectro-spatial covariance pattern would be a promising tool for personalized monitoring and management of neurodegenerative diseases.

Limitations

There are some limitations in our study. Firstly, the use of EEG data collected from two different EEG recording devices due to a device change may have affected the data quality and characteristics. To address this issue, we employed relative band power, a more robust measure compared to absolute band power. However, it is worth noting that using absolute band power could yield different spatial characteristics compared to the pattern obtained in the study.

Secondly, it is important to note that EEG records cortical activity, and signals from subcortical structures are too weak to be properly captured. Many regions known to contribute significantly to PD or DLB related brain metabolism are located in subcortical structures, and their contributions may not be fully represented in our EEG patterns since we constrained the source space to the cortical surface.

Additionally, there was no correlation between MoCA-K scores and pattern expression after adjusting age and sex. To better evaluate the relationship between cognitive function and pattern expression, future studies should include more subjects within similar age ranges, encompassing varying degrees of cognitive

impairment. Moreover, using subtest scores instead of the total score in cognitive assessments could provide a more detailed examination of the relationship with specific cognitive functions.

Furthermore, we did not conduct a follow-up on the HC group. Incorporating follow-up data on the HC group could have allowed us to isolate the effects of normal aging from the effects of diseases.

Conclusion

Our study is the first to identify EEG spectro-spatial covariance pattern related to PD and DLB preceding iRBD and observe longitudinal trajectories of PD, DLB, and iRBD nonconverters. Utilizing EEG spectro-spatial covariance patterns in combination with patterns from other modalities would provide a more comprehensive understanding of phenoconversion in iRBD patients.

Bibliography

1. Postuma RB, Iranzo A, Hu M, et al. Risk and predictors of dementia and parkinsonism in idiopathic REM sleep behaviour disorder: a multicentre study. *Brain*. 2019;142(3):744-759. doi:10.1093/brain/awz030

2. Schenck CH, Bundlie SR, Mahowald MW. Delayed emergence of a parkinsonian disorder in 38% of 29 older men initially diagnosed with idiopathic rapid eye movement sleep behavior disorder. *Neurology*. 1996;46(2):388-393. doi:10.1212/WNL.46.2.388

3. Zhou J, Zhang J, Lam SP, Tang X, Wing YK. Clinical Biomarkers of Neurodegeneration in REM Sleep Behavior Disorder. *J Sleep Med*. 2015;12(2):27-33. doi:10.13078/jsm.15006

4. Spetsieris P, Ma Y, Peng S, et al. Identification of Disease-related Spatial Covariance Patterns using Neuroimaging Data. *Journal of visualized experiments : JoVE*. July 2013. doi:10.3791/50319

5. Ma Y, Tang C, Spetsieris PG, Dhawan V, Eidelberg D. Abnormal Metabolic Network Activity in Parkinson'S Disease: Test—Retest Reproducibility. *J Cereb Blood Flow Metab*. 2007;27(3):597-605. doi:10.1038/sj.jcbfm.9600358

6. Shin JH, Lee JY, Kim YK, et al. Parkinson Disease-Related Brain Metabolic Patterns and Neurodegeneration in Isolated REM Sleep Behavior Disorder. *Neurology*. 2021;97(4):e378-e388. doi:10.1212/WNL.0000000000012228

7. Perovnik M, Tomše P, Jamšek J, Tang C, Eidelberg D, Trošt M. Metabolic brain pattern in dementia with Lewy bodies: Relationship to Alzheimer's disease topography. *NeuroImage: Clinical*. 2022;35:103080. doi:10.1016/j.nicl.2022.103080

8. Yoon EJ, Lee JY, Nam H, et al. A New Metabolic Network Correlated with Olfactory and Executive Dysfunctions in Idiopathic Rapid Eye Movement Sleep Behavior Disorder. *Journal of Clinical Neurology*. 2019;15(2):175-183. doi:10.3988/jcn.2019.15.2.175

9. Shin JH, Kim H, Kim YK, et al. Longitudinal evolution of cortical thickness signature reflecting Lewy body dementia in isolated REM sleep behavior disorder: a prospective cohort study. *Translational Neurodegeneration*. 2023;12(1):27. doi:10.1186/s40035-023-00356-y

10. Kim R, Lee JY, Kim YK, et al. Longitudinal Changes in Isolated Rapid Eye Movement Sleep Behavior Disorder-Related Metabolic Pattern Expression. *Movement Disorders*. 2021;36(8):1889-1898. doi:10.1002/mds.28592

11. Livia Fantini M, Gagnon JF, Petit D, et al. Slowing of electroencephalogram in rapid eye movement sleep behavior disorder. *Annals of Neurology*. 2003;53(6):774-780. doi:10.1002/ana.10547

12. Rodrigues Brazète J, Montplaisir J, Petit D, et al. Electroencephalogram slowing in rapid eye movement sleep behavior disorder is associated with mild cognitive impairment. *Sleep Medicine*. 2013;14(11):1059-1063. doi:10.1016/j.sleep.2013.06.013

13. Rodrigues Brazète J, Gagnon JF, Postuma RB, Bertrand JA, Petit D, Montplaisir J. Electroencephalogram slowing predicts neurodegeneration in rapid eye movement sleep behavior disorder. *Neurobiology of Aging*. 2016;37:74-81. doi:10.1016/j.neurobiolaging.2015.10.007

14. Stoffers D, Bosboom JLW, Deijen JB, Wolters EC, Berendse HW, Stam CJ. Slowing of oscillatory brain activity is a stable characteristic of Parkinson's disease without dementia. *Brain*. 2007;130(7):1847-1860. doi:10.1093/brain/awm034

15. American Academy of Sleep Medicine. *The International Classification of Sleep Disorders*. 3rd ed. Dalien, IL; 2014.

16. Hughes AJ, Daniel SE, Kilford L, Lees AJ. Accuracy of clinical diagnosis of idiopathic Parkinson's disease: a clinico-pathological study of 100 cases. *Journal of Neurology, Neurosurgery & Psychiatry*. 1992;55(3):181-184. doi:10.1136/jnnp.55.3.181

17. McKeith IG, Boeve BF, Dickson DW, et al. Diagnosis and management of dementia with Lewy bodies: Fourth consensus report of the DLB Consortium. *Neurology*. 2017;89(1):88-100. doi:10.1212/WNL.0000000000004058

18. Gilman S, Wenning GK, Low PA, et al. Second consensus statement on the diagnosis of multiple system atrophy. *Neurology*. 2008;71(9):670-676. doi:10.1212/01.wnl.0000324625.00404.15

19. Jung TP, Makeig S, Humphries C, et al. Removing electroencephalographic artifacts by blind source separation. *Psychophysiology*. 2000;37(2):163-178. doi:10.1111/1469-8986.3720163

20. Pion-Tonachini L, Kreutz-Delgado K, Makeig S. ICLabel: An automated electroencephalographic independent component classifier, dataset, and website. *NeuroImage*. 2019;198:181-197. doi:10.1016/j.neuroimage.2019.05.026

21. Delorme A, Makeig S. EEGLAB: an open source toolbox for analysis of

single-trial EEG dynamics including independent component analysis. *Journal of Neuroscience Methods*. 2004;134(1):9-21. doi:10.1016/j.jneumeth.2003.10.009

22. Pascual-Marqui RD. Standardized low-resolution brain electromagnetic tomography (sLORETA): technical details. *Methods Find Exp Clin Pharmacol*. 2002;24 Suppl D:5-12.

23. Tadel F, Baillet S, Mosher JC, Pantazis D, Leahy RM. Brainstorm: A User-Friendly Application for MEG/EEG Analysis. *Computational Intelligence and Neuroscience*. 2011;2011:e879716. doi:10.1155/2011/879716

24. Destrieux C, Fischl B, Dale A, Halgren E. Automatic parcellation of human cortical gyri and sulci using standard anatomical nomenclature. *NeuroImage*. 2010;53(1):1-15. doi:10.1016/j.neuroimage.2010.06.010

25. Teune LK, Renken RJ, Mudali D, et al. Validation of parkinsonian disease-related metabolic brain patterns. *Movement Disorders*. 2013;28(4):547-551. doi:10.1002/mds.25361

26. Meles SK, Kok JG, De Jong BM, et al. The cerebral metabolic topography of spinocerebellar ataxia type 3. *NeuroImage: Clinical*. 2018;19:90-97. doi:10.1016/j.nicl.2018.03.038

27. Meles SK, Renken RJ, Pagani M, et al. Abnormal pattern of brain glucose metabolism in Parkinson's disease: replication in three European cohorts. *Eur J Nucl Med Mol Imaging*. 2020;47(2):437-450. doi:10.1007/s00259-019-04570-7

28. Morbelli S, Chincarini A, Brendel M, et al. Metabolic patterns across core features in dementia with lewy bodies. *Annals of Neurology*. 2019;85(5):715-725. doi:10.1002/ana.25453

29. Meles SK, Renken RJ, Janzen A, et al. The Metabolic Pattern of Idiopathic REM Sleep Behavior Disorder Reflects Early-Stage Parkinson Disease. *Journal of Nuclear Medicine*. 2018;59(9):1437-1444. doi:10.2967/jnumed.117.202242

30. Wu P, Yu H, Peng S, et al. Consistent abnormalities in metabolic network activity in idiopathic rapid eye movement sleep behaviour disorder. *Brain*. 2014;137(12):3122-3128. doi:10.1093/brain/awu290

31. Iranzo A, Isetta V, Molinuevo JL, et al. Electroencephalographic slowing heralds mild cognitive impairment in idiopathic REM sleep behavior disorder. *Sleep Medicine*. 2010;11(6):534-539. doi:10.1016/j.sleep.2010.03.006

32. Massicotte-Marquez J, Décary A, Gagnon JF, et al. Executive dysfunction and memory impairment in idiopathic REM sleep behavior disorder. *Neurology*. 2008;70(15):1250-1257. doi:10.1212/01.wnl.0000286943.79593.a6

33. Lu J, Ge J, Chen K, et al. Consistent Abnormalities in Metabolic Patterns of Lewy Body Dementias. *Movement Disorders*. 2022;37(9):1861-1871. doi:10.1002/mds.29138

34. van der Zande JJ, Gouw AA, van Steenoven I, Scheltens P, Stam CJ, Lemstra AW. EEG Characteristics of Dementia With Lewy Bodies, Alzheimer's Disease and Mixed Pathology. *Frontiers in Aging Neuroscience*. 2018;10. https://www.frontiersin.org/articles/10.3389/fnagi.2018.00190. Accessed March 2, 2023.

35. Latreille V, Carrier J, Gaudet-Fex B, et al. Electroencephalographic prodromal markers of dementia across conscious states in Parkinson's disease. *Brain*. 2016;139(4):1189-1199. doi:10.1093/brain/aww018

36. Nakamura A, Cuesta P, Fernández A, et al. Electromagnetic signatures of the preclinical and prodromal stages of Alzheimer's disease. *Brain*. 2018;141(5):1470-1485. doi:10.1093/brain/awy044

37. Mattioli P, Orso B, Liguori C, et al. Derivation and Validation of a Phenoconversion-Related Pattern in Idiopathic Rapid Eye Movement Behavior Disorder. *Movement Disorders*. 2023;38(1):57-67. doi:10.1002/mds.29236

38. Gaubert S, Raimondo F, Houot M, et al. EEG evidence of compensatory mechanisms in preclinical Alzheimer's disease. *Brain*. 2019;142(7):2096-2112. doi:10.1093/brain/awz150

39. Jeong E, Cha KS, Shin HR, et al. Alerting network alteration in isolated rapid eye movement sleep behavior disorder patients with mild cognitive impairment. *Sleep Medicine*. 2022;89:10-18. doi:10.1016/j.sleep.2021.11.002

40. Chang KH, French IT, Liang WK, et al. Evaluating the Different Stages of Parkinson's Disease Using Electroencephalography With Holo-Hilbert Spectral Analysis. *Front Aging Neurosci*. 2022;14. doi:10.3389/fnagi.2022.832637

41. Pal A, Pegwal N, Behari M, Sharma R. High delta and gamma EEG power in resting state characterise dementia in Parkinson's patients. *Biomarkers in Neuropsychiatry*. 2020;3:100027. doi:10.1016/j.bionps.2020.100027

국문 초록

연구 배경: 본 연구에서는 단독 렘수면행동장애(iRBD) 환자에서 신경퇴행질환으로 전환되는 것과 관련이 있는 뇌파 주파수-공간 공분산 패턴을 규명하고, iRBD 환자와 파킨슨병(PD)환자, 루이소체치매(DLB) 환자들에서 변화 궤적을 조사하는 것을 목표로 하였다.

연구 방법: PD로 전환된 12명, DLB로 전환된 6명, 추적기간 동안 전환되지 않은 iRBD 환자 17명으로부터 눈을 감은 상태의 휴지기 뇌파를 기준선과 추적 시점에서 수집하였다. PD나 DLB로 전환된 이후에 수집된 뇌파 데이터와 나이와 성별이 짝지어진 12명의 건강 대조군(HC)의 뇌파 데이터를 사용하여 소스 공간에서 PD로 전환된 iRBD(PD-RBD), DLB로 전환된 iRBD(DLB-RBD)과 관련된 패턴을 각 주파수 밴드에 대해서 얻었다. 패턴 발현 점수와 운동기능, 인지기능을 측정한 점수 간의 상관관계를 분석하였다. 또한 기준선에서 신경퇴행질환으로 전환된 환자와 그렇지 않은 환자 간에 패턴발현점수의 차이가 있는 지 확인하였다. 마지막으로, 패턴을 조합하여 만든 공간에서 질병전환이 되지 않은 iRBD 환자와 PD로 전환된 환자, DLB로 전환된 환자의 변화 궤적을 각각 관찰하였다.

연구 결과: 델타, 알파밴드의 공분산 패턴이 PD나 DLB로 전환된 환자를 HC로부터 효과적으로 구분하였으며, 알파밴드 패턴이 가장 높은 구분력을 보였다(수신자 동작 특성 곡선 아래 면적(AUC)=0.9097 (PD-RBD 알파 패턴), AUC = 0.9306 (DLB-RBD 알파 패턴)). 운동기능을 반영하는 MDS-UPDRS part III 점수는 나이와 성별을 보정 한 후에도 델타밴드 패턴의 점수와 양의 상관관계가 있었다(스피어만 상관계수(rho)=0.688, p=0.00014 (PD-RBD 델타 패턴), rho=0.539, p=0.0055 (DLB-RBD 델타 패턴)). 그러나 인지기능을 반영하는 MoCA-K 점수는 어떠한 패턴의 점수와도 유의미한 상관관계가 발견되지 않았다. 기준선에서 추후에 질병전환된 환자들의 PD-RBD와 DLB-RBD 베타2 패턴의 점수가 전환되지 않은 환자에 비해 모두 높았으나, 두 집단이 잘 분리되지는 않았다(AUC=0.7751, 순위합 검정 p=0.0062). 세 집단 모두 조합된 패턴 공간에서 오른쪽으로 이동하는 공통적인 변화 궤적을 보였고, 각 집단의 종적 궤적에서 구분되는 특징도 존재하였다.

결론: PD-RBD, DLB-RBD 관련 뇌파 주파수-공간 공분산 패턴은

신경퇴행질환의 조기 감지와 질병 모니터링에 활용될 수 있을 것으로 기대된다. 다른 형태의 데이터에서 얻은 패턴과 상보적으로 사용된다면 iRBD에서 일어나는 질병전환의 메커니즘을 이해하는 데 도움이 될 것이다.

주요어 : 렘수면행동장애; 뇌파; 알파-시누클레인병증; 파킨슨병; 루이소체 치매; 공간 공분산 패턴.
학 번 : 2021-23744